OPEN ACCESS
JOURNAL OF ADVANCED DIELECTRICS
Vol. 14, No. 3 (2024) 2440011 (6 pages)

DOI: 10.1142/S2010135X24400113

Enhanced energy-storage performance with optimized thermally stable dielectric property in BNT–BST ceramics modified by KNN doping

Shurong Li*, Chenglong Zhang*, Suzhi Li*, Le Zhang†,‡ and Haijun Wu*,§
*State Key Laboratory for Mechanical Behavior of Materials
Xi'an Jiaotong University, 710049, Xi'an, P. R. China

†School of Physics, Xi'an Jiaotong University, 710049, Xi'an, P. R. China
‡le.zhang@xjtu.edu.cn
§wuhaijunnavy@xjtu.edu.cn

Received 13 April 2024; Revised 5 May 2024; Accepted 13 May 2024; Published 21 June 2024

Developing environmental-friendly materials with high-density energy storage is of paramount importance to meet the burgeoning demands for energy storage. In this study, we harness the modulation of a multicomponent solid solution by introducing KNN as a third element into the BNT–BST system, thereby achieving a marked enhancement in both energy storage performance and the temperature stability of the dielectric constant. BNBST–4KNN stands out for its exceptional dielectric stability, with a dielectric constant variation rate within 10% across a broad temperature range of 40°C to 400°C, a feat attributed to the flattening and broadening of the T_m peak. BNBT–2KNN exhibits superior energy storage capabilities, with an energy storage density of 1.324 J/cm^3 and an energy storage efficiency of 72.3%, a result of the P–E loop becoming more slender. These advancements are pivotal for the sustainable progression of energy storage technologies.

Keywords: BNT; energy storage; dielectric.

1. Introduction

High-density energy storage materials enable the compact containment of greater energy reserves, effectively addressing the escalating requirements for power retention and bolstering the deployment of cutting-edge technological innovations.[1–5] Consequently, the deployment of high-density energy storage materials plays a pivotal role in driving the evolution of electronic devices towards miniaturization, enhanced efficiency, and extended battery life.[6] Dielectric capacitors are ideal candidates for the next generation of energy storage materials attributed to their outstanding performance including rapid charge–discharge rates, substantial power density, enduring operational lifespan, and an expansive range of working temperatures.[1,7,8]

For an extended period, lead-based materials, exemplified by PZT, have maintained a dominant role in the commercial domain of ferroelectric ceramics, which is attributed to their superior piezoelectric coefficients, robust dielectric properties, and advantageous electromechanical coupling characteristics, underpinned by the sophistication of their associated technological and industrial infrastructures.[9–13] Nonetheless, the utilization of lead-based materials entails considerable risks to human health and the environment during recycling and secondary utilization processes.[14] Consequently, the European Union has promulgated the Restriction of Hazardous Substances (RoHS) directive, which imposes restrictions on the incorporation of lead-containing materials in electronic components, thereby addressing the imperative for environmentally benign alternatives.[15–17] Therefore, there is an urgent need to develop a new class of environmentally friendly, lead-free dielectric ceramics to mitigate the ecological and health risks associated with traditional lead-containing materials.

Sodium bismuth titanate ($Bi_{0.5}Na_{0.5}TiO_3$, BNT) ceramics, endowed with a notably high maximum polarization intensity (P_m) have emerged as a focal point of research within the realm of dielectric energy storage.[10,18–20] Nevertheless, the BNT-based ceramics exhibit a relatively high level of residual polarization (P_r) and a significant coercive field (E_c), characteristics that are detrimental to the enhancement of their energy storage capabilities.[15,21–23] Researchers have incorporated a second element $Bi_{0.2}Sr_{0.7}TiO_3$ (BST) into Barium Titanate (BNT), leading to a reduction in the values of P_r and E_c, while maintaining the P_m. This strategic modification has yielded an optimized profile for energy storage performance.[3,13,24,25]

In this study, the incorporation of $K_{0.5}Na_{0.5}NbO_3$ into the $0.7Bi_{0.5}Na_{0.5}TiO_3$–$0.3\ Bi_{0.2}Sr_{0.7}TiO_3$ binary system has been explored, resulting in a significant enhancement of both energy storage performance and dielectric properties.

§Corresponding author.

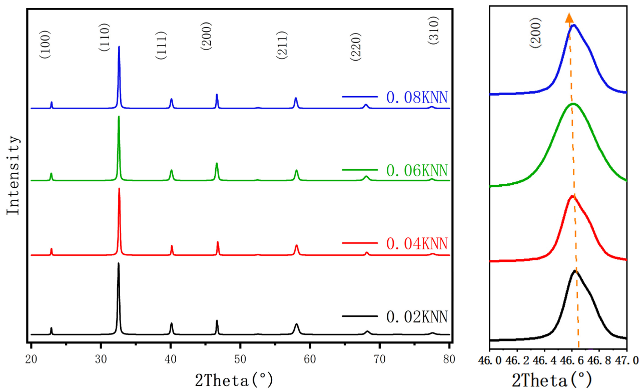

Fig. 1. XRD results of BNBST-xKNN.

2. Experimental Results

$(1-x)(0.7Bi_{0.5}Na_{0.5}TiO_3$–$0.3Bi_{0.2}Sr_{0.7}TiO_3)$–$xK_{0.5}Na_{0.5}NbO_3$ ceramics (abbreviated as BNBST–xKNN, x = 0–0.08) were prepared by solid-state reaction method, employing Bi_2O_3 (99.99%, alfa), Na_2CO_3 (99.5%, alfa), Tio_2 (99.8%, alfa), $SrCO_3$ (99%, alfa), K_2CO_3 (99%, alfa) and Nb_2O_5 (99.9%, alfa) as starting raw materials. Initially, the raw materials weighed according to the stoichiometric formula, were thoroughly mixed using a wet ball-milling technique to ensure homogeneity. Then, the dried powders were calcined at 850°C for 6 h. After ball milling again, they were subsequently mixed with 5% PVA to facilitate consolidation. Finally, they were compacted into pellets, which were finally sintered at 1150–1175°C for 2 h.

3. Result and Discussion

The powder X-ray diffraction (XRD) results of BNBST–xKNN are shown in Fig. 1.

The X-ray diffraction (XRD) analysis reveals that all specimens exhibit a single perovskite phase, without detectable impurity peaks, indicating that the third-element, KNN, has been fully dissolved into the lattice of the BNTBST matrix. The absence of peak shifts or splitting in the XRD patterns suggests that all samples possess a pseudocubic structure, which implies that the incorporation of KNN has not induced any long-range noncubic distortions.[26]

Figure 2 illustrates the temperature-dependent variations of the dielectric permittivity (ε_r) and loss ($\tan\delta$) for the BNBST–xKNN samples. The testing was performed at temperatures from room temperature to 450°C, with a heating rate of 3°C per minute, and the testing frequencies included 0.1 kHz, 1 kHz, 10 kHz, 100 kHz, and 1000 kHz. The dielectric constant serves as a measure of a material's response to an electric field, characterizing its capacity to store energy within the field, and holds significant reference value for the study of energy storage performance. The curve reveals that

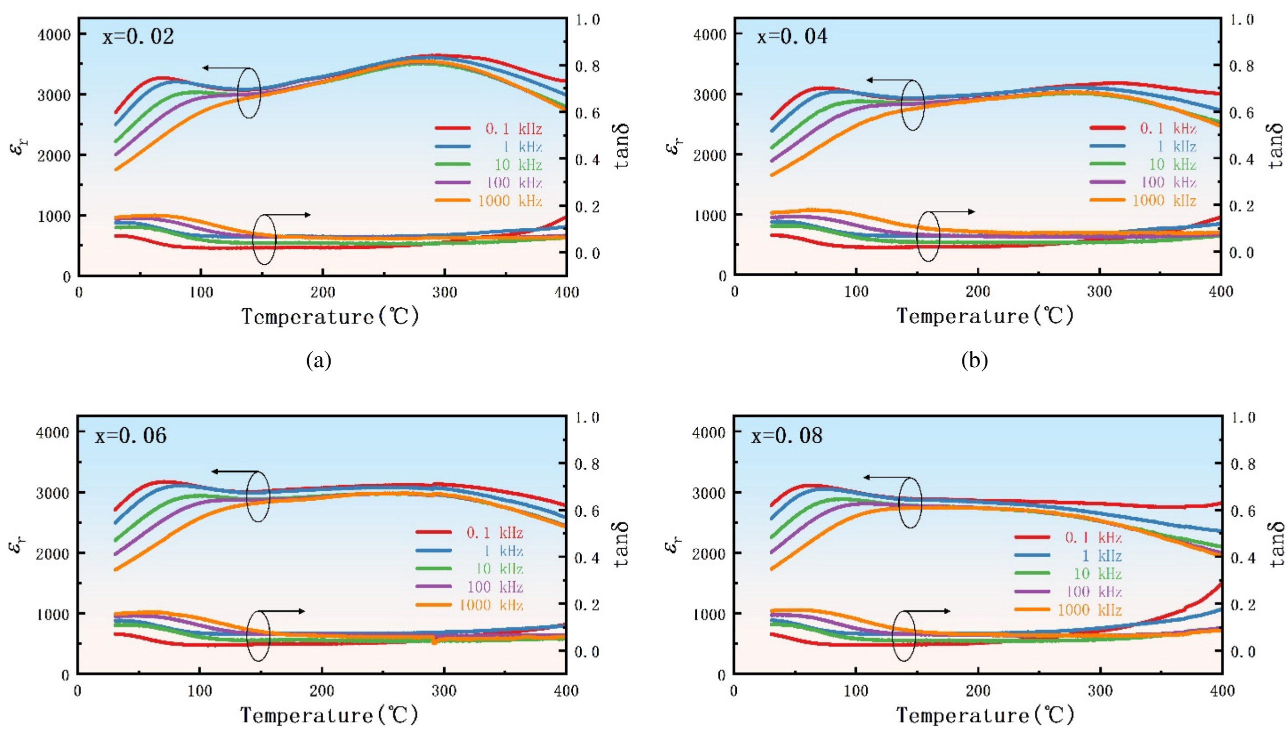

(a) (b) (c) (d)

Fig. 2. Dielectric permittivity and loss of BNBST–xKNN: (a–d) $x = 0.02$–0.08.

all BNBST–xKNN specimens exhibit two anomalous dielectric peaks at T_s and T_m, which are characteristic of relaxor ferroelectrics, signifying the complex dielectric behavior typical of such materials. While the temperature below the T_s, the ε_r–T (dielectric permittivity–temperature) curve exhibits a pronounced frequency dispersion phenomenon. This behavior is associated with the thermal activation process of polar nanoregions (PNRs), rather than a phase transition process. It is commonly accepted that below a certain temperature, the thermodynamic behavior of polar nanoregions becomes relatively static, and this temperature is referred to as the freezing temperature, denoted as T_f. The freezing temperature (T_f) is determined through fitting to the Vogel–Fulcher formula:

$$f = f_0 \cdot \exp\left[-\frac{E_a}{k} \cdot (T_m - T_f)\right], \tag{1}$$

where f_0 is the Debye frequency, E_a is the thermodynamic activation energy, and k is the Boltzmann constant. Figure 3 presents the fitted freezing temperatures for samples of all compositions. From the figure, it can be observed that the freezing temperatures for all samples are in the vicinity of room temperature, indicating that the nanoscale ferroelectric domains within the BNBST–KNN system are in a highly active state at ambient conditions. Furthermore, the freezing temperature progressively shifts towards lower temperature as the doping concentration increases. The observed phenomenon may be ascribed to the substitutional incorporation of KNN into the crystal lattice, which perturbs the lattice structure and compromises the long-range order of the BNBST matrix, consequently augmenting the relaxor characteristics. The secondary dielectric peak is associated with the Curie temperature, signifying the culmination of the phase transition from the rhombohedral to the tetragonal phase. Examination of the figure reveals that the incorporation of KNN does not effect a displacement of the T_m dielectric peak. Nonetheless, this modification is associated with an observed broadening of the peak.

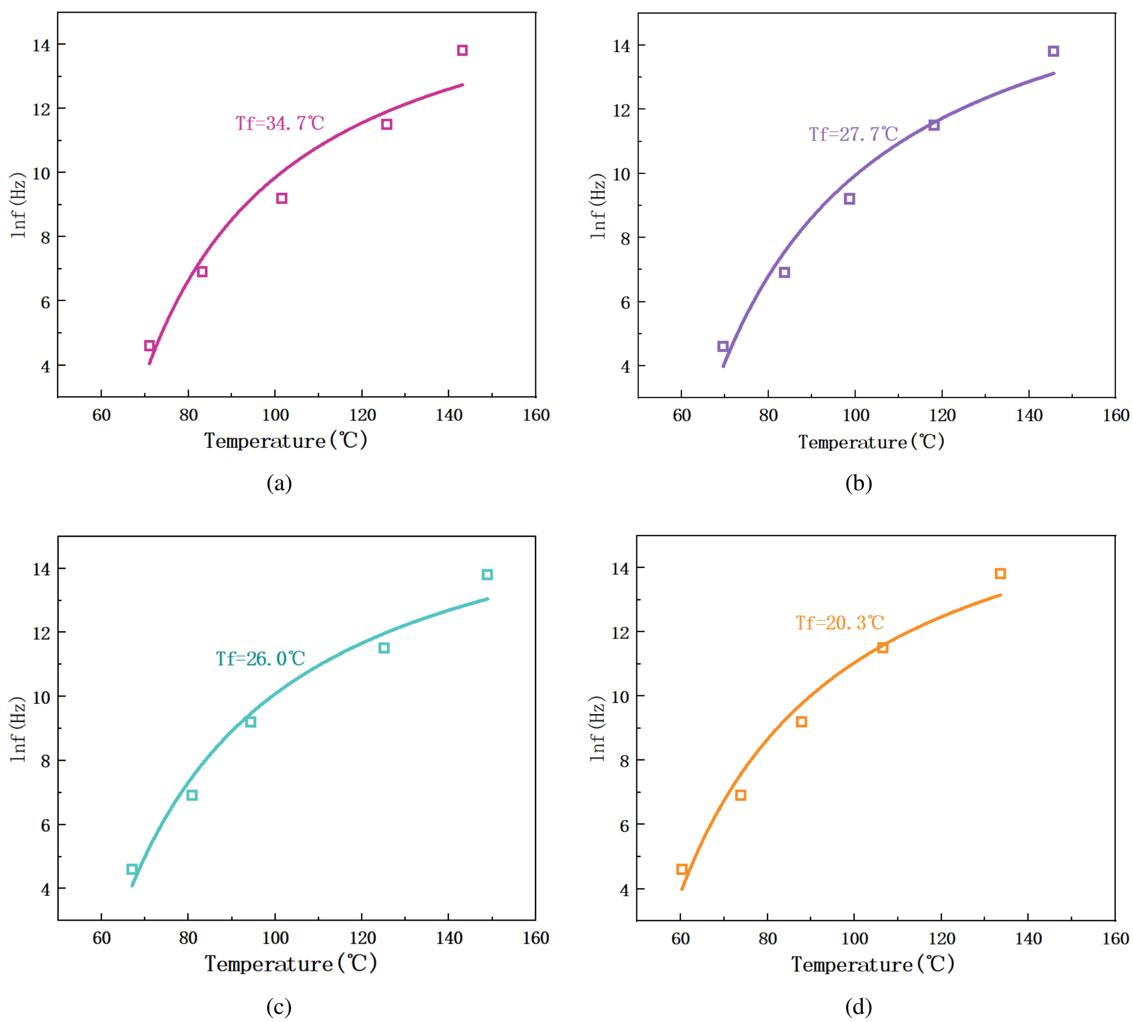

Fig. 3. The fitted freezing temperatures of BNBST–xKNN: (a–d) $x = 0.02$–0.08.

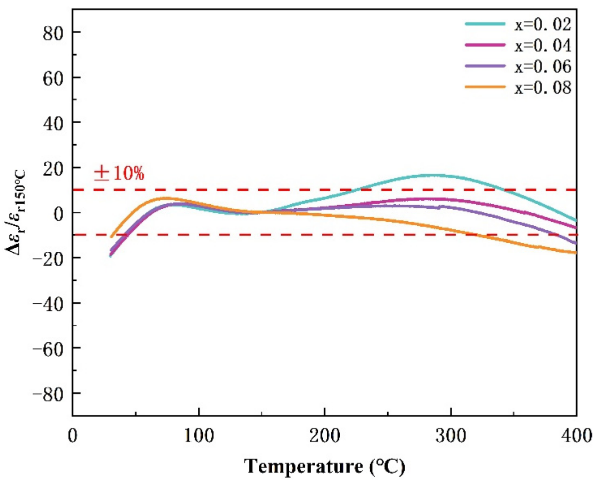

Fig. 4. Temperature stability of dielectric constants of BNBST–xKNN.

The thermal stability of the dielectric constant is typically characterized by the expression $\Delta\varepsilon/\varepsilon 150^{\circ}$C, which signifies the assessment of the material's dielectric performance stability with respect to temperature fluctuations, focusing on the rate of change of the dielectric constant at the reference temperature of 150°C. Figure 4 displays the temperature stability of dielectric constants under 1 kHz of BNBST–xKNN over the entire measured temperature range. The region shaded in red delineates the scope wherein the variation rate is constrained to a range of 10%. The figure suggests that the temperature stability range expands progressively with an increment in the quantity of KNN. Within the temperature interval of 40–400°C, the dielectric constant of the BNBST–4KNN ceramic exhibits the most pronounced stability. The enhancement of dielectric temperature stability has a significant impact on the assessment of energy storage performance at medium to high temperatures. It is conducive to the development of medium to high temperature energy storage medium ceramics with excellent energy storage density, suitable for application fields with higher operating temperatures, such as oil and gas exploration and hybrid automobile engines.

Figure 5 presents the ferroelectric ($P-E$) loops of the BNBST–xKNN specimens at a testing frequency of 10 Hz and variation of P_m and P_r with composition. Figure 5(a) illustrates the transitions from an originally waist-like shape to a more slim profile. Figure 5(b) demonstrates that with the increase of KNN doping concentration, both P_r and P_m exhibit a significant reduction. Notably, P_r approaches nearly zero. Based on the computational equations derived from energy storage density, these slim hysteresis loops indicate the suitability of these materials for energy storage applications. The corresponding mathematical equations are given as follows:

$$W = \int_0^{P_{\max}} E dP, \tag{2}$$

$$W_{\text{rec}} = \int_{P_r}^{P_{\max}} E dP, \tag{3}$$

$$\eta = \frac{W_{\text{rec}}}{W_{\text{rec}} + W_{\text{loss}}} \times 100\%. \tag{4}$$

It can be observed that the saturation polarization intensity decreases from 41 μC/cm^2 in BNBST to 29 μC/cm^2 in BNBST–8KNN, representing a reduction of 29.2%. Concurrently, the remanent polarization intensity diminishes from 5.4 μC/cm^2 to 2.6 μC/cm^2, indicating a decrease of 51.8%. The primary factors contributing to the degradation of ferroelectric properties and the reduction of P_r are generally attributed to the lattice distortions induced by the incorporation of KNN, which disrupts the long-range order of the BNBST matrix and enhances the local structural disorder in

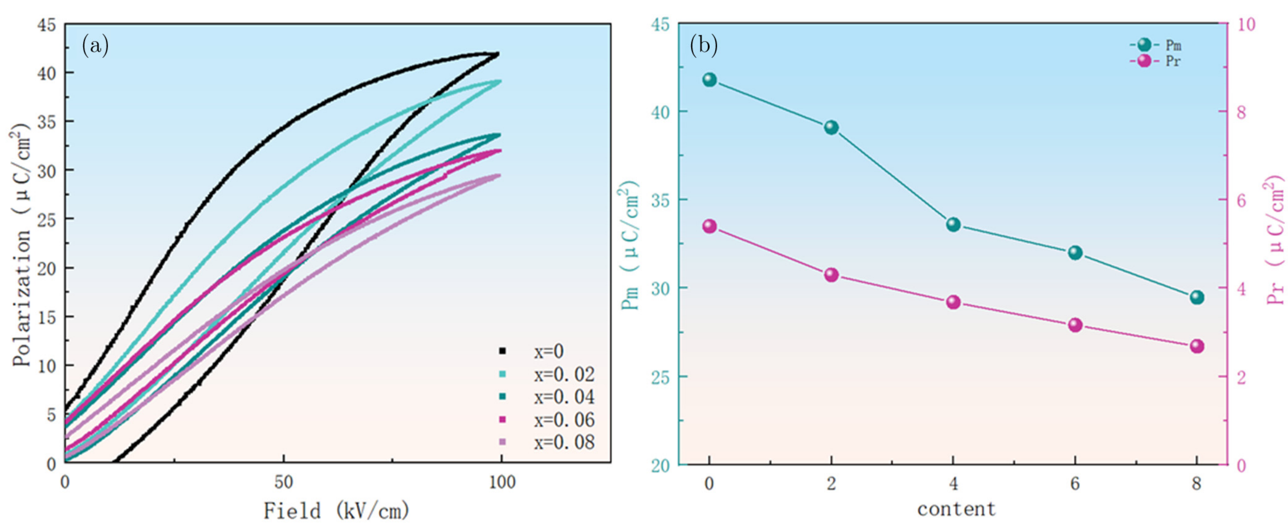

Fig. 5. (a) P–E loops of BNBST–xKNN, (b) variation of P_m and P_r with composition.

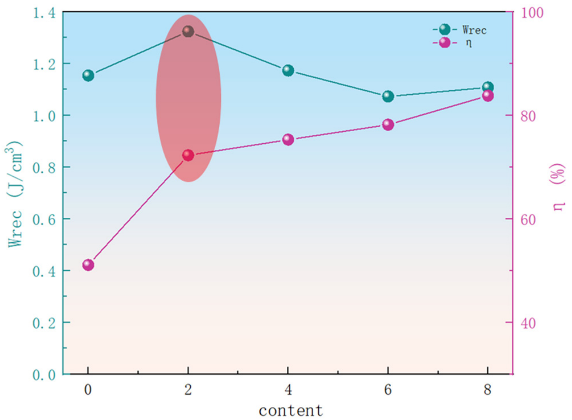

Fig. 6. Energy storage densities and efficiency of BNBST–xKNN.

the ceramic samples, thereby undermining the ferroelectricity. This phenomenon leads to an increased degree of relaxation, heightened thermodynamic activity of Polar Nanoregions (PNRs), and a propensity for nanoscale ferroelectric domains within the material to arrange disorderly in various directions under the influence of an electric field. Consequently, this affects the field-induced transition process of PNRs to macroscopic domains. As the KNN content escalates, the transition becomes increasingly challenging, culminating in a decrement in both P_m and the energy storage density. Furthermore, an increase in KNN content is accompanied by a marginal decline in the P_r (remanent polarization) values, which mitigates energy dissipation within the material and enhances the energy storage efficiency.

Figure 6 displays the energy storage density and storage efficiency of the BNBST-xKNN ceramics. Examination of the figure reveals that as the doping concentration is incremented, the energy storage density exhibits an initial ascent followed by a subsequent descent, achieving a peak value of 1.324 J/cm^3 at $x = 0.02$, which represents a significant enhancement of 15% relative to the pristine matrix. In accordance with the formula governing energy storage density, a high value of W_{rec} is contingent upon a combination of elevated saturation polarization and diminished remanent polarization. Consequently, the maximization of W_{rec} at a doping concentration of 0.02 is attributed to the rate at which the saturation polarization decreases being less pronounced than that of the remanent polarization. Upon further escalation of the doping concentration, there is a precipitous decline in the saturation polarization intensity, while the remanent polarization intensity exhibits no significant alteration, thereby culminating in a diminution of the energy storage density. According to the formula for calculating energy storage efficiency, a lower energy loss density (W_{loss}) corresponds to a higher storage efficiency. The energy loss density (W_{loss}) represents the portion of energy that cannot be fully released due to the presence of remanent polarization (P_r). Consequently, as the doping concentration is incremented, the remanent polarization intensity progressively diminishes, resulting in a monotonic ascent in the energy storage efficiency. Overall, the BNBST–xKNN ceramics exhibits optimal performance at $x = 0.02$, as it concurrently possesses both a high energy storage density and efficiency.

4. Conclusion

In this study, BNBST–xKNN ceramics were designed and synthesized utilizing the solid-state reaction method. A series of investigations have demonstrated that an optimal level of KNN doping can significantly enhance the dielectric stability and energy storage performance of the modified ceramics. The BNBST–4KNN demonstrated a variation rate of the dielectric constant below 10% across the temperature range of 40°C to 400°C, which exhibits exemplary temperature stability of the dielectric constant. This is predominantly ascribed to the introduction of KNN into the system, which leads to the amelioration and expansion of the T_m peak. The BNT–2KNN composite demonstrates enhanced energy storage capabilities, achieving an energy storage density of 1.324 J/cm^3 and an energy storage efficiency of 72.3%. These values represent significant improvements over the base matrix, with respective increases of 15% and 41.5%. The enhancements are attributed to the increased optimal values of P_m and P_r.

Acknowledgments

The authors would like to acknowledge the financial support from the National Key R&D Program of China (2021YFB3201100) and the National Natural Science Foundation of China (52172128). The authors would like to thank the strong support from the Instrumental Analysis Center of Xi'an Jiaotong University.

ORCID

Haijun Wu https://orcid.org/0000-0002-7303-379X

References

[1] X. Fang et al., Low-field-driven superior energy storage effect with excellent thermal stability by constructing coexistent glasses, *ACS Appl. Mater. Interf.* **16**, 11497 (2024).
[2] P. Gao et al., New antiferroelectric perovskite system with ultrahigh energy-storage performance at low electric field, *Chem. Mater.* **31**(3), 979 (2019).
[3] D. Li et al., Achieved ultrahigh energy storage properties and outstanding charge–discharge performances in $(Na_{0.5}Bi_{0.5})0.7$ $Sr_{0.3}TiO_3$-based ceramics by introducing a linear additive, *Chem. Eng. J.* **392**, 123729 (2020).
[4] J. Lin et al., Simultaneously achieving high performance of energy storage and transparency via A-site non-stoichiometric defect engineering in KNN-based ceramics, *Chem. Eng. J.* **444**, 136538 (2022).
[5] H. Palneedi et al., High-performance dielectric ceramic films for energy storage capacitors: progress and outlook, *Adv. Funct. Mater.* **28**(42), 1803665 (2018).

[6]L. Liu *et al.*, Achieving high energy storage performance and ultrafast discharge speed in $SrTiO_3$-based ceramics via a synergistic effect of chemical modification and defect chemistry, *Chem. Eng. J.* **429**, 132548 (2022).
[7]X. Ren *et al.*, Achieving high energy storage density and excellent stability in $BiScO_3$ modified $BaTiO_3$-based ceramics, *Ceram. Int.* **50**(5), 8109 (2024).
[8]Y. Huang *et al.*, Thermal stability of dielectric and energy storage performances of Ca-substituted BNTZ ferroelectric ceramics, *Ceram. Int.* **47**, 6298 (2021).
[9]W. Zhu *et al.*, A review:(Bi, Na) TiO_3 (BNT)-based energy storage ceramics, *J. Mater.* (2023).
[10]D. Jain ruth *et al.*, Enhanced electrical properties in Rb-substituted sodium bismuth titanate ceramics, *Appl. Phys. A* **122**, 1 (2016).
[11]X. Zhou *et al.*, Investigation of structural and electrical properties of B-site complex Ion (Mg 1/3 Nb 2/3) 4+-modified high-Curie-temperature $BiFeO_3$-$BaTiO_3$ ceramics, *J. Electron. Mater.* **43**, 755 (2014).
[12]Y. Xu *et al.*, High energy storage properties of lead-free Mn-doped (1-x) $AgNbO_3$-$xBi_{0.5}Na_{0.5}TiO_3$ antiferroelectric ceramics, *J. Eur. Ceram. Soc.* **40**(1) 56 (2020).
[13]C. Xu *et al.*, High charge-discharge performance of $Pb_{0.98}La_{0.02}$ $(Zr_{0.35}Sn_{0.55}Ti_{0.10})$ 0.995 O_3 antiferroelectric ceramics, *J. Appl. Phys.* **120**(7) (2016).
[14]K. R. Muhammed *et al.*, Physical properties and sinterability of pure and iron-doped bismuth sodium titanate ceramics, *J. Austr. Ceram. Soc.* **56**, 1441 (2020).
[15]Y. Shen *et al.*, Constructing novel binary $Bi_{0.5}Na_{0.5}TiO_3$-based composite ceramics for excellent energy storage performances via defect engineering, *Chem. Eng. J.* **439**, 135762 (2022).
[16]M.-H. Zhang *et al.*, Review on field-induced phase transitions in lead-free $NaNbO_3$-based antiferroelectric perovskite oxides for energy storage, *J. Materiom.* **9**(1), 1 (2023).
[17]Z. Sun *et al.*, Progress, outlook, and challenges in lead-free energy-storage ferroelectrics, *Adv. Electron. Mater.* **6**(1), 1900698 (2020).
[18]T. Oh and M.-H. Kim, Phase relation and dielectric properties in (Bi1/2 Na1/2) 1− x Bax TiO_3 TiO_3 lead-free ceramics, *Mater. Sci. Eng. B* **132**(3), 239 (2006).
[19]R. Cheng *et al.*, Investigation of structural and electrical properties of B-site complex ion (Nd1/2 Ta1/2) 4+-doped Bi 1/2 Na 1/2 TiO_3 lead-free piezoelectric ceramic, *J. Mater. Sci. Mater. Electron.* **26**, 5409 (2015).
[20]F. Li *et al.*, Local structural heterogeneity and electromechanical responses of ferroelectrics: learning from relaxor ferroelectrics, *Adv. Funct. Mater.* **28**(37), 1801504 (2018).
[21]Z. Pan *et al.*, Achieving high discharge energy density and efficiency with NBT-based ceramics for application in capacitors, *J. Mater. Chem. C* **7**(14), 4072 (2019).
[22]Y. Pu *et al.*, High energy storage density and optical transparency of microwave sintered homogeneous $(Na_{0.5}Bi_{0.5})$ $(1-x)$ Bax Ti $(1-y)$ $SnyO_3$ ceramics, *ACS Sust. Chem. Eng.* **6**(5), 6102 (2018).
[23]X. Qiao *et al.*, $Bi_{0.5}$ $Na_{0.5}$ TiO_3-based relaxor ferroelectric ceramic with large energy density and high efficiency under a moderate electric field, *J. Mater. Chem. C* **7**(34), 10514 (2019).
[24]K. Yao *et al.*, $Bi_{0.5}$ $Na_{0.5}TiO_3$–$Sr_{0.85}Bi_{0.1}TiO_3$ ceramics with high energy storage properties and extremely fast discharge speed via regulating relaxation temperature, *Ceram. Int.* **47**(8), 11294 (2021).
[25]S.-E. Park and K. S. Hong, Variations of structure and dielectric properties on substituting A-site cations for Sr2+ in (Na1/2Bi1/2) TiO_3, *J. Mater. Res.* **12**(8), 2152 (1997).
[26]A. Rachakom, S. Jiansirisomboon and A. Watcharapasorn, Effect of poling on piezoelectric and ferroelectric properties of $Bi_{0.5}Na_{0.5}Ti_{1-x}ZrxO_3$ ceramics, *J. Electroceram.* **33**, 105 (2014).